IMPROVEMENTS IN MODAL PARAMETER EXTRACTION THROUGH POST-PROCESSING FREQUENCY RESPONSE FUNCTION ESTIMATES

Berke M. Gur
Prof. Christopher Niezrecki
Prof. Peter Avitabile
Structural Dynamics and Acoustic Systems Laboratory
University of Massachusetts Lowell

ABSTRACT

Frequency response functions are the primary means of experimentally evaluating the structural characteristics of dynamic systems. These response functions, which are frequently utilized in vibration and modal analysis, are estimated through the periodograms of measurements. Some form of averaging of the periodograms is necessary to eliminate the effects of unavoidable estimation and measurement noise. In the last decade, wavelet domain denoising methods have emerged as powerful means of estimating functions from noisy data. As an application of these methods in structural dynamics, wavelet domain denoising methods and their variants have recently been proposed as a post processor step for reducing the number of averaging operations required in frequency response function estimation. In this paper, the improvements in modal parameter estimates resulting from median interpolating transform post-processing of periodograms are investigated through an analytical test case. It is shown that the number of required averages can significantly be reduced when periodograms and the median interpolating pyramid transform are implemented together. The improvements in modal parameter estimates for a fixed number of averages are quantified in terms of bias and variance.

INTRODUCTION

FRFs are the frequency domain equivalent of a system's impulse response relating the system inputs to the outputs. FRFs are the primary means of representing the response characteristics of dynamic systems and are widely used in vibration [1] and modal analysis [2]. In practice, FRFs are calculated from a finite set of input and output measurements through spectral estimators. Although various spectral estimators have been developed in the signal processing literature [3], the periodogram estimator is by far the most popular due to its efficiency and low computational cost. Practical difficulties related to FRF calculation are the inconsistency of the periodogram estimator and the high sensitivity of the FRFs to measurement errors made in the input and output of the system. The most popular method of reducing estimation variance and noise contamination is to average the periodograms obtained from a several sets of measurements. The required number of averages, and thus measurement interval, increases as measurement noise becomes more significant. This increased sampling interval not only increases the computational load, but can also result in the violation of the LTI system assumption. An alternate to time averaging is to post process the periodograms using some noise reduction scheme.

In the last decade, the wavelet transform has been proposed as a post processor step for eliminating noise contamination in FRFs. Bodin and Wahlberg assumed identically and independently distributed (i.i.d.) Gaussian measurement noise at the output only and analyzed wavelet coefficient shrinkage denoising of FRFs obtained through Blackman-Tukey PSD estimates using a Hann window [4]. While wavelet domain denoising methods are near optimal in eliminating Gaussian noise, their denoising performance suffers if the noise is heavy tailed. It can be shown that FRFs are generally corrupted with non-Gaussian noise, even if random measurement errors are made at the output only. When measurement errors are made in both the outputs and inputs, the resulting FRF is contaminated with impulsive noise. Kim *et al*. pointed to the existence of this impulsive noise in FRF estimates and suggested denoising FRFs through a combination of median filtering and wavelet denoising, known as the RWD algorithm [5]. However, in Reference [5], noise reduction is evaluated in terms of the FRF waveform, rather than the modal parameters which have more practical significance. Recently, Gur and Niezrecki [6] implemented a MIPT based coefficient shrinkage algorithm, developed by Donoho and Yu [7] for post processing of noisy FRFs.

This paper builds upon the results presented in [6]. In particular, MIPT based post-processing is evaluated in terms of accuracy in the extracted modal parameters. The algorithm is tested on a simple 2 DOF analytic model with known modal

parameters. The estimation errors in modal parameters extracted from periodograms with and without post-processing are numerically evaluated and compared through Monte-Carlo simulations.

THEORY AND PROPOSED METHOD

Classical Spectral FRF Estimation:

The FRF of a LTI system is defined as the Fourier transform of the system impulse response. The FRF is calculated as the ratio of the cross- and auto-PSD of the output and input

$$H(f) = \frac{P_{yx}(f)}{P_{xx}(f)}, \tag{1}$$

where the PSD is the expectation of the DFT squared of a signal

$$P_{xx}(f) = \lim_{M\to\infty} E\left\{\frac{1}{2M+1}\left|\sum_{n=-M}^{M} w(n)x(n)\exp(-j2\pi fn)\right|^2\right\}, \tag{2}$$

and $w(n)$ is a window function. The PSD can be estimated through either parametric or non-parametric methods. The periodogram

$$\hat{P}_{xx}(f) = \frac{1}{N}\left|\sum_{n=0}^{N-1} w(n)x(n)\exp(-j2\pi fn)\right|^2, \tag{3}$$

is a very efficient estimator of the PSD where N represents the number of samples used for the estimate. It can be shown that the periodogram is an asymptotically unbiased but inconsistent estimator

$$\lim_{N\to\infty} E[\hat{P}_{xx}(f)] = P_{xx}(f), \quad \text{var}[\hat{P}_{xx}(f)] \approx P_{xx}^2(f). \tag{4}$$

From Eq. (4) it is observed that the uncertainty associated with the periodogram estimates is of the order of the estimate itself, indicating a poor estimator performance. This inconsistency and poor performance of the periodogram is attributed to elimination of the expectation operator in going from Eq. (2) to Eq. (3). In an effort to reduce the variance of the periodogram, the Welch periodogram divides the available N data samples into K, possibly overlapping, clusters, each with L samples. The PSD is estimated through averaging the K periodograms, each obtained using L data samples. For non-overlapping data samples, the variance of the periodogram reduces to [3]

$$\text{var}[\hat{P}_{xx,aver}(f)] \approx \frac{1}{K}\text{var}\left[\sum_{m=0}^{K-1} P_{xx}^{(m)}(f)\right]. \tag{5}$$

Without the loss of generality, normalized frequencies are assumed such that $0 \le f < 1$ in the remainder of this paper.

Effects of Measurement Noise on FRF Estimates

FRFs are very sensitive to measurement noise and noisy measurements can severely affect the modal parameter estimates. In this paper, measurement noise is modeled as zero mean Gaussian signals $v(t) \sim \mathcal{N}(0,\sigma_v^2)$, and $w(t) \sim \mathcal{N}(0,\sigma_w^2)$ superposed to the system outputs and inputs, respectively

$$Z(f) = H(f)U(f) + H(f)W(f) + V(f), \tag{6}$$

where $Z(f)$, $U(f)$, $W(f)$, and $V(f)$ are the DFT's of noisy output measurements, inputs, and input output measurement noise signals, respectively.

While modeling random measurement errors as a zero mean Gaussian process is a reasonable assumption, the resulting noise in the FRFs is highly impulsive and cannot be modeled as additive Gaussian noise. As pointed out in [5] and from empirical observations, FRF noise is modeled as non-Gaussian, impulsive noise. In particular, the SαS distribution is a viable candidate for modeling FRF noise. Both the Gaussian and the heavier tailed Cauchy distributions are special cases of SαS distributions.

Wavelet Domain Noise Reduction

Wavelet transforms have attracted significant interest in the last decade due to their ability to selectively process noisy functions at various resolutions. Through this selective processing, noise reduction can be accomplished while preserving very fine details of a function. The DWT of the FRF estimate $\hat{H}$ is defined as the integral transform

$$\{\mathcal{W}\hat{H}\}(j,k) = \int_0^1 \hat{H}(\xi) 2^{-j/2} \psi(2^{-j}\xi - k) d\xi, \tag{7}$$

where $\psi(\xi)$, j and k are the wavelet basis function, scale and translation variables, respectively. Wavelet domain noise reduction is accomplished by a forward transform, followed by a non-linear thresholding. It is assumed that the function samples get mapped as a few very large amplitude coefficients while noise is mapped as small amplitude coefficients. The noise free signal is obtained through an inverse DWT of the thresholded coefficients. This mapping is very effective when noise is Gaussian and it has been shown that classical wavelet domain denoising methods achieve near optimal performance for functions of certain smoothness classes [8]. However, these methods breakdown when noise contamination is much more impulsive compared to Gaussian noise, as coefficients due to impulsive noise get mapped as high amplitude coefficients and elude thresholding.

Robust Wavelet Denoising

The RWD is similar to DWT based algorithms except for a median filtering stage imposed on approximate coefficients. The approximate coefficients, to which impulsive noise is likely to leak, is subtracted from their median. If the coefficient is due to impulsive noise, then this difference will be large. Therefore, a soft threshold is applied to this difference between the coefficients and the median. As a result of this threshold, the impulsive noise coefficients are likely to pass unaffected. Subtracting these thresholded differences from the actual approximate coefficients eliminates impulsive noise components, for an appropriate selection of the threshold. The detail coefficients are thresholded as in the case of the DWT to eliminate Gaussian noise. Thus, the RWD is capable of eliminating both impulsive noise and Gaussian noise, through median filtering and classical wavelet thresholding, respectively.

Median Interpolating Pyramid Transform Thresholding

The MIPT based denoising method developed in Reference [7] also consists of three stages. The forward transform maps the signal to the transform domain, followed by a thresholding operation to eliminate the coefficients due to noise. The noise-free signal is recovered through an inverse MIPT. However, the algorithm is significantly different than traditional wavelet based methods in the way it maps the FRF to a new domain where denoising is to be performed. Rather than using basis functions, the MIPT proceeds by calculating the medians of triadic groups of samples of the FRF

$$m_{j,k} = \text{median}[\hat{H}(f)], \quad f \in I_{j,k} = [k \cdot 3^{-j}, (k+1) \cdot 3^{-j}), \tag{8}$$

where $j \geq 0$ is a non-negative integer representing the scale variable, and $0 \leq k < 3^j$ is the non-negative integer representing translation variable. Using the median of the function at a point indexed by (j,k) in the time-scale space and two adjacent medians, the MIPT fits a quadratic polynomial $\pi_{j,k}(f) = a_{j,k} + b_{j,k} f + c_{j,k} f^2$ whose median matches these medians

$$\begin{aligned} &\text{median}[\pi_{j,k}(f)] = m_{j,k-1}, \quad f \in I_{j,k-1}, \\ &\text{median}[\pi_{j,k}(f)] = m_{j,k}, \quad f \in I_{j,k}, \\ &\text{median}[\pi_{j,k}(f)] = m_{j,k+1}, \quad f \in I_{j,k+1}. \end{aligned} \tag{9}$$

In Reference [7], it is shown that despite being a nonlinear operator, the median of a quadratic polynomial can analytically be obtained in terms of its extremum. Based on this analytic expression of the median, and the set of three equations given in Eq. (9), one can solve for the coefficients $a_{j,k}$, $b_{j,k}$, and $c_{j,k}$. The medians of the function at the next finer resolution about the time index k are predicted from this quadratic polynomial

$$\begin{aligned} \tilde{m}_{j+1,3k} &= \text{median}[\pi_{j,k}(f)], \quad f \in I_{j,3k}, \\ \tilde{m}_{j+1,3k+1} &= \text{median}[\pi_{j,k}(f)], \quad f \in I_{j,3k+1}, \\ \tilde{m}_{j+1,3k+2} &= \text{median}[\pi_{j,k}(f)], \quad f \in I_{j,3k+2}. \end{aligned} \tag{10}$$

Similar to the last stage of the median filtering of the RWD algorithm, the difference between the actual medians $m_{j,k}$ and the estimates $\tilde{m}_{j,k}$ is said to be the transform coefficients $\alpha_{j,k}$ at a given scale j and translation k

$$\alpha_{j,k} = m_{j,k} - \tilde{m}_{j,k}. \tag{11}$$

This polynomial construction, median estimation and coefficient calculation sequence is repeated until a predefined cut-off scale j_0 is reached. The coefficients at this final terminal scale j_0 are set to the medians for this scale (i.e., $m_{j_0,k}$). The MIPT results in a vector of coefficients

$$\boldsymbol{\theta} = [\mathbf{m}_{j_0}^T \quad \boldsymbol{\alpha}_{j_0+1}^T \quad \cdots \quad \boldsymbol{\alpha}_J^T]^T, \tag{12}$$

where $\mathbf{m}_{j_0}(k) = m_{j_0,k}, \quad 0 \le k < 3^{j_0}$ and $\boldsymbol{\alpha}_j(k) = \alpha_{j,k}, \quad 0 \le k < 3^j$.

A hard threshold is imposed on the normalized coefficients $\bar{\alpha}_{j,k} = 3^{(J-j)/2}\alpha_{j,k}$

$$\delta_\eta^h(\bar{\alpha}_{j,k}) = \begin{cases} \bar{\alpha}_{j,k}, & |\bar{\alpha}_{j,k}| \ge \eta_j, \\ 0, & |\bar{\alpha}_{j,k}| < \eta_j, \end{cases} \tag{13}$$

where $\boldsymbol{\eta} = [\eta_{j_0+1} \quad \eta_{j_0+2} \quad \cdots \quad \eta_J]^T$ is a vector of scale dependent thresholds. The thresholds are determined through asymptotic properties of random variables. Similar to the thresholds developed for classical wavelet denoising methods, it is desirable to find a threshold η_j such that the probability of the MIPT coefficients due to i.i.d. noise exceeding this threshold asymptotically approaches zero

$$\lim_{N\to\infty} \Pr(|\bar{\alpha}_{j,k}| > \eta_j) \to 0. \tag{14}$$

When noise can be characterized through a symmetric probability distribution $F_v(v)$, this threshold is shown to be

$$\eta_j = 3^{(J-j)/2} F_v^{-1}(\xi), \quad \xi = 1/2 + \left[1 - (2J3^J)^{-2/(3^{J-j})}\right]^{1/2}/2. \tag{15}$$

Most SαS distributions do not possess an analytic distribution function, and Eq. (15) cannot be solved explicitly to obtain a threshold. However, the contribution of the distribution to the threshold does not vary significantly at the course scales for different SαS distributions. Therefore, the thresholds for SαS noise distributions can be estimated through the thresholds for SαS distributions that possess analytical distribution functions. Gaussian or Cauchy distributions are suitable candidates for this purpose. For results presented in this paper, the Cauchy CDF is used. After elimination of the coefficients due to noise through hard thresholding, the noise free estimate of the function is obtained by reconstruction of the remaining coefficients through the inverse MIPT. Detailed discussions related to the MIPT, the inverse MIPT, the properties and implementation of the MIPT and the thresholds can be found in Reference [7].

SIMULATION RESULTS AND DICUSSIONS

In this section, the MIPT post processing algorithm is evaluated in terms of the accuracy in the modal parameter extraction using a simple, 2 DOF analytic system defined by

$$\mathbf{G}(s) = \frac{\begin{bmatrix} G_{11}(s) & G_{12}(s) \\ G_{21}(s) & G_{22}(s) \end{bmatrix}}{(s+50 \pm j579.06)(s+50 \pm j787.96)}, \tag{16}$$

where

$$\begin{aligned} G_{11}(s) &= s^2 + 100s + 532800, \quad & G_{12}(s) &= 132900, \\ G_{21}(s) &= 132900, & G_{22}(s) &= s^2 + 100s + 428400. \end{aligned} \tag{17}$$

The above MIMO transfer function is discretized at a sampling rate of 400 Hz for computer simulation. In Reference [6], estimation of FRFs from magnitude and phase information is considered. In this paper, real and imaginary representations of FRFs are preferred based on empirical evidence suggesting more robust FRF noise reduction performance of the MIPT algorithm. In particular, this is improvement in performance is due to the oscillations that inherently exist in the vicinity of sharp discontinuities (i.e., in phase FRF data) following the truncation of the data (i.e., thresholding). Although the discontinuities can be avoided through unwrapping the phase, it is more convenient to work with real-imaginary FRF pairs. The real and imaginary parts of the FRF $H_{11}(f)$ between output $X_1(f)$ and input $U_1(f)$ are analytically calculated and plotted in Figure 1.

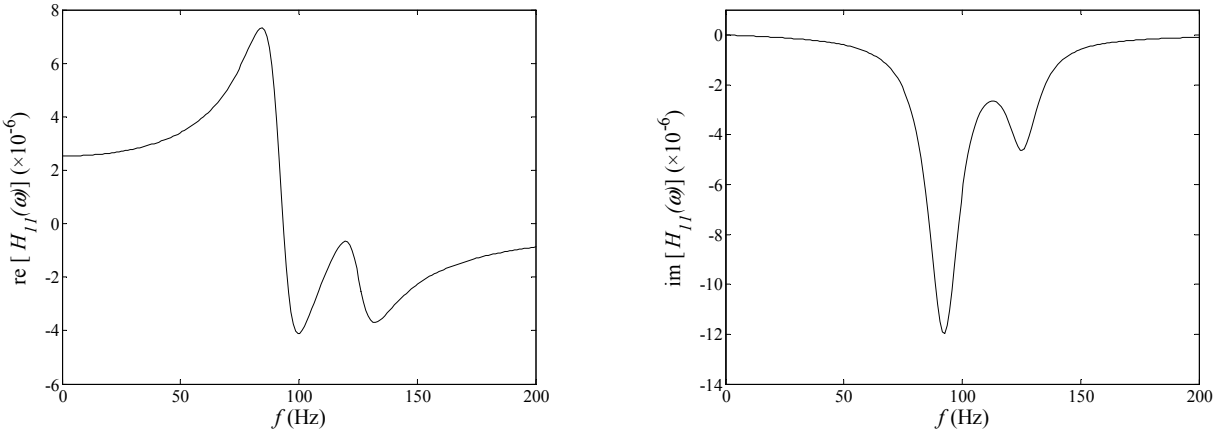

Figure 1 The real (left) and imaginary (right) parts of the analytically calculated FRF H_{11}.

The H_{11} system is excited with zero mean, unit variance random inputs of 4372 samples. Random measurement noise is introduced to both the inputs and outputs such that the SNR is 20 dB and 35 dB, respectively. These SNRs correspond to measurement errors of the order of 10% and 1% peak signal amplitude. A typical realization of the system input and output signals and their associated measurement noise are plotted in Figure 2. The resulting impulsive noise contamination on the single periodogram FRF estimates are shown in Figure 3. The noise contamination on these FRFs is due to the combined effect of estimation variance and measurement noise at the inputs and outputs.

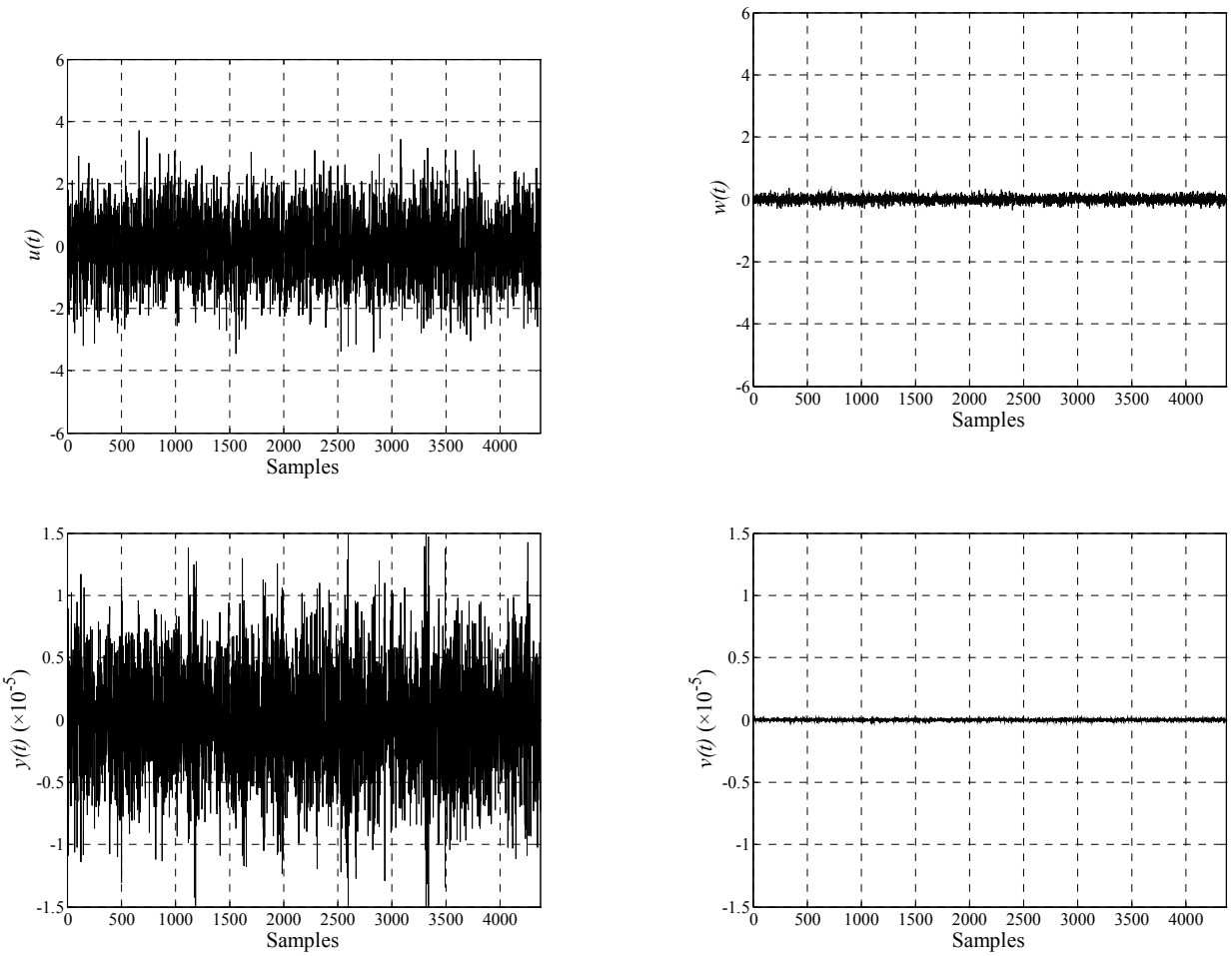

Figure 2 The system input (top, left) and output (bottom, left) signals, and their corresponding measurement errors (top, right) and (bottom, right).

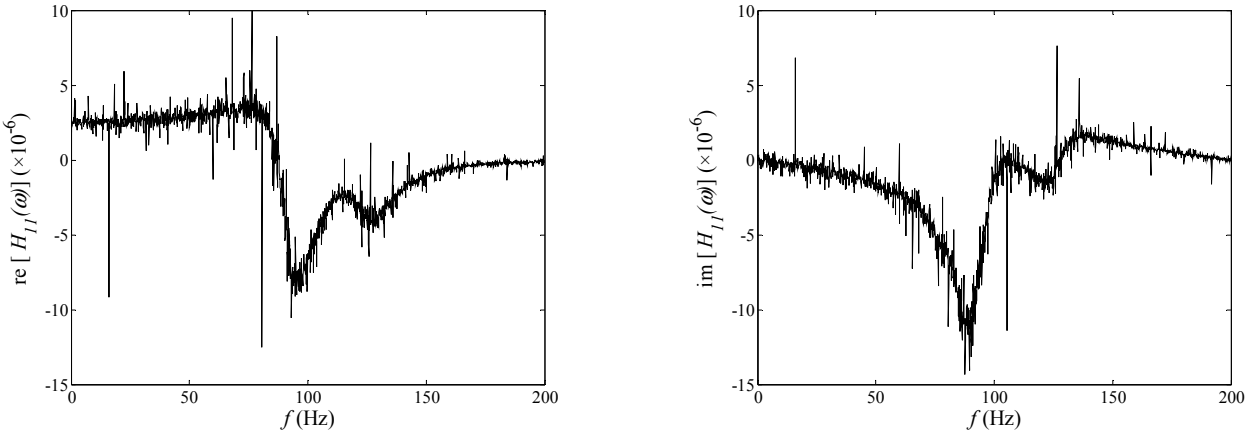

Figure 3 The real (left) and imaginary (right) parts of the single periodogram estimate of $\hat{H}_{11}$ obtained from a noisy set of measurements.

In the MIPT algorithm, the 4372 samples results in $J = 7$ levels, but the two most course resolutions are not thresholded (i.e., $j_0 = 5$). As with the ordinary periodogram estimates, the post-processed FRFs are averaged. Up to 40 averages are performed to eliminate the noise contamination on the FRFs. Following each averaging operation, the modal parameters are extracted from the FRF estimates using the Vibrant Technology ME'scope v4.0 vibration analysis software [9]. In Figure 4, the frequency, damping, and residue estimates are plotted as a function of the number of averages for both the ordinary periodogram estimates and the MIPT post-processed estimates.

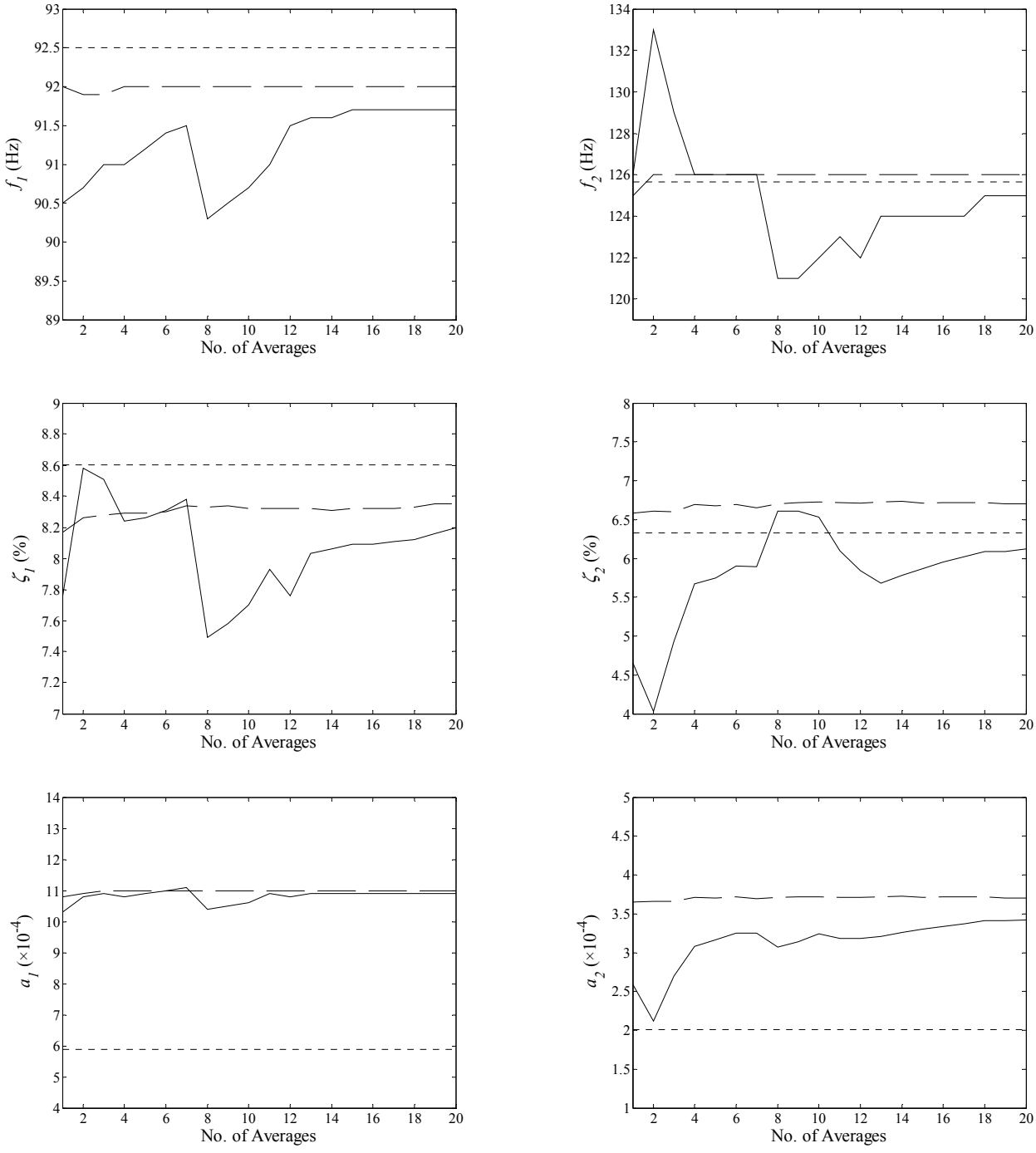

Figure 4 The convergence of the modal parameter estimates from averaged periodograms (dashed), and averaged MIPT post-processed periodograms (solid) versus the analytic parameters (dotted) for resonant frequencies (top), for damping ratios (middle), and for residues (bottom).

Modal parameter estimates from MIPT post-processed FRFs converge within several averages, while the ordinary periodogram averaging based FRFs require more than 20 averages for convergence in most cases. Both sets of estimates are biased, not only due to the fact that finite sample estimates have been used, but also due to distortion resulting from windowing. In Figure 5, the final FRF estimates obtained from 40 averages are plotted.

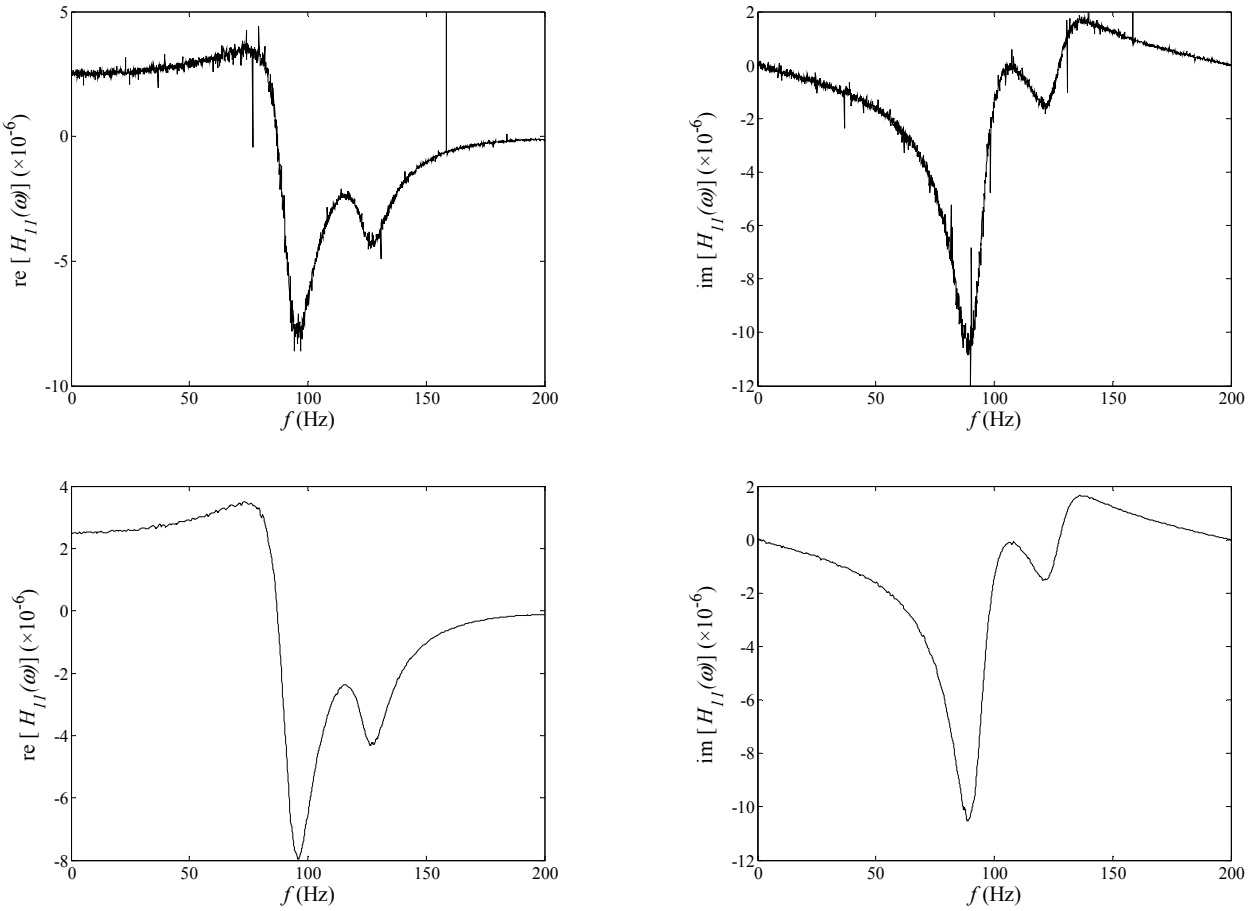

Figure 5 The real and imaginary FRF estimates resulting from 40 averages using ordinary periodograms (top), and MIPT post-processed periodograms (bottom).

The convergence and consistency of the MIPT post-processed periodograms are evaluated though 100 Monte-Carlo simulations and compared to ordinary averaged periodogram estimates. Mean values of the estimated parameters and the associated bias and variance in the estimates are shown in Tables I, II, and III, respectively.

Table I Mean value of the modal parameter estimates before and after MIPT post-processing.

Parameter Estimates						
	f1 (Hz)	f2 (Hz)	ζ1 (%)	ζ2 (%)	|a1|	|a2|
Periodogram	91.2	125.7	8.0	6.2	5.302E-04	1.836E-04
MIPT	92.1	126.0	8.3	6.7	5.491E-04	1.859E-04

Table II Bias in of the modal parameter estimates before and after MIPT post-processing.

Bias						
	f1 (Hz)	f2 (Hz)	ζ1 (%)	ζ2 (%)	|a1|	|a2|
Periodogram	-1.3	0.1	-0.6	-0.1	-5.884E-05	-1.741E-05
MIPT	-0.4	0.3	-0.3	0.4	-3.990E-05	-1.510E-05

Table III Variance in the parameter estimates before and after MIPT post-processing.

Variance						
	f1 (Hz)	f2 (Hz)	ζ1 (%)	ζ2 (%)	|a1|	|a2|
Periodogram	2.7	71.7	1.2	1.7	5.197041E-09	2.795473E-08
MIPT	0.0	0.0	0.0	0.0	6.252525E-12	4.129293E-11

MIPT can be viewed as a post-processing filter that performs non-linear smoothing of the FRFs. Similar to windowing, this will inevitably cause distortion in the FRFs. The effects of this distortion can be quantified in Table II, where MIPT post-processing increases the bias on the estimates for some parameters. This is not an unexpected result since the periodogram is an asymptotically unbiased estimator. However, examining the estimation variances given in Table III, one can conclude that this unbiasedness has little significance when each Monte-Carlo simulation is considered individually. The relatively very low variances associated with the MIPT post-processing suggest that these estimates, while being slightly off from the true parameters, are significantly consistent and more reliable than the averaged periodogram results. This consistency is demonstrated in Figure 6 where we plot a typical FRF realization from the Monte-Carlo trials.

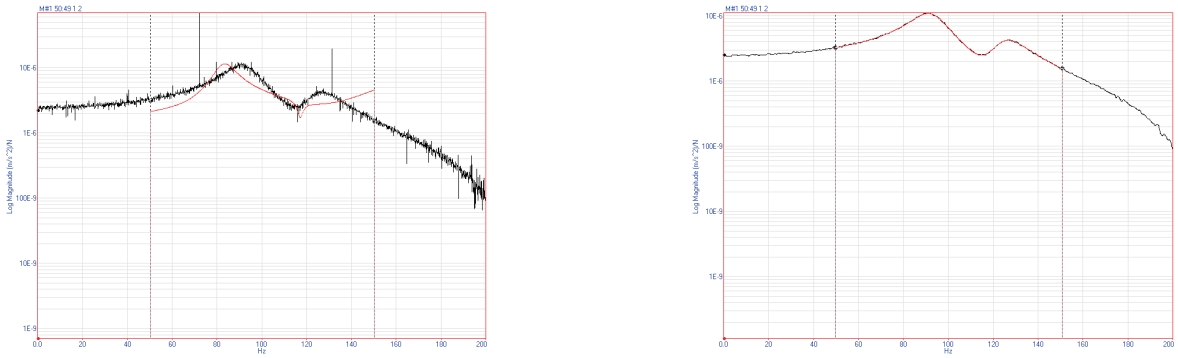

Figure 6 The magnitude FRF estimates resulting from 10 averages using ordinary periodograms (left, in black), and MIPT post-processed periodograms (right, in black) superposed by the curve fits obtained in ME'scope VES (red).

Impulsive noise on appearing on averaged periodogram based estimates prevents accurate modal parameter extraction., while a very accurate fit has been obtained for the MIPT post-processed periodograms. The fit interval is arbitrarily selected between 50 and 150 Hz. However, shrinking the fit interval further degrades modal parameter estimates due to the presence of the impulse around the 125.7 Hz peak. The analytically obtained parameters and the parameter estimates for this realization are given in Table IV.

Table IV Analytically obtained parameters and a single realization parameters estimates before and after MIPT post-processing.

	Single Realization Parameter Estimates					
	f1 (Hz)	f2 (Hz)	ζ1 (%)	ζ2 (%)	|a1|	|a2|
Analytic	92.5	125.7	8.60	6.33	5.890E-04	2.010E-04
Periodogram	82.9	117.0	6.03	1.85	3.095E-04	2.010E-05
MIPT	92.1	125.0	8.58	6.38	5.700E-04	1.805E-04

CONCLUSIONS AND FUTURE WORK

In this paper, improvements in modal parameter estimation through MIPT post processing of the FRFs are evaluated. Using a simple analytic model, it is demonstrated that the MIPT algorithm offers significant reduction in the number of periodogram averages required to achieve a given accuracy in parameter estimates. Although magnitude-phase information can be used in MIPT based denoising of FRFs, post processing of real-imaginary FRFs have proven to be more robust, and thus used in this paper. One disadvantage of the MIPT is that it operates on triadic datasets while the FFT based periodogram is most efficiently implemented in dyadic orders. However, through simulations, it is shown that the MIPT is a very effective method for eliminating impulsive noise on FRFs and can improve modal parameter estimates when only a limited number of noisy measurements are available. As a follow up to the work presented in this paper, the MIPT based denoising algorithm are being tested on experimental vibration data. These results will be published in future papers.

NOTATION

Acronyms

FRF	Frequency Response Function
PSD	Power Spectral Density

MIPT	Median Interpolating Pyramid Transform
DWT	Discrete Wavelet Transform
RWD	Robust Wavelet Transform
SαS	Symmetric Alpha Stable
CDF	Cumulative Distribution Function

REFERENCES

1 Meirovitch, L., *Principles and Techniques of Vibrations*, Prentice Hall, Upper Saddle River, NJ, (1997).
2 Kobayashi, A. S., *Handbook of Experimental Mechanics*, Prentice Hall, Upper Saddle River, NJ (1987).
3 Kay, S. M., *Modern Spectral Estimation: Theory and Applications* Prentice-Hall, Upper Saddle River, New Jersey, (1988).
4 Bodin, P., and Wahlberg, B, "A frequency response estimation method based on smoothing and thresholding," International Journal of Adaptive Control and Signal Processing, 12, 407-416 (1998).
5 Kim, Y. Y., Hong, J.-C., and Lee, N.-Y., "Frequency response functions estimation via a robust wavelet de-noising method," Journal of Sound and Vibration, 244(4), 635-649 (2001).
6 Gur, B. M., and Niezrecki, C., "Non-linear median transform domain denoising of frequency response functions," *Proc. of 36th InterNoise Conf.*, Istanbul, Turkey (2007).
7 Donoho, D. L., and Yu, T. P.-Y., "Nonlinear pyramid transforms based on median-interpolation," SIAM Journal on Mathematical Analysis, 31(5), 1030-1061 (2000).
8 Donoho, D. L., "De-noising by soft-thresholding," IEEE Transactions on Information Theory, 41(3), 613-627 (1995).
9 Vibrant Technology, Inc., 5 Erba Lane, Suite B Scotts Valley, CA 95066.